


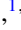



Enhancing high harmonic generation in GaAs by elliptically polarized light excitationFumiya Sekiguchi ^{1,*},[†] Minoru Sakamoto,^{1,*} Kotaro Nakagawa,¹ Hirokazu Tahara ^{1,2} Shunsuke A. Sato ^{3,4}
Hideki Hirori ^{1,‡} and Yoshihiko Kanemitsu ^{1,§}¹*Institute for Chemical Research, Kyoto University, Uji, Kyoto 611-0011, Japan*²*The Hakubi Center for Advanced Research, Kyoto University, Kyoto 606-8501, Japan*³*Center for Computational Sciences, University of Tsukuba, Tsukuba 305-8577, Japan*⁴*Max Planck Institute for the Structure and Dynamics of Matter, Luruper Chaussee 149, 22761 Hamburg, Germany*

(Received 24 April 2023; accepted 26 October 2023; published 13 November 2023)

Reflecting crystal and electronic structures, high harmonic generation (HHG) in solids show intriguing behaviors that are absent in isotropic gases, and are expected to be novel light sources and spectroscopic tools. Recent studies reported that the efficiency of HHG in some materials can be enhanced by using elliptically polarized excitations, which we call “elliptical enhancement”, while the mechanism underlying the phenomenon remains unknown. Here, we unambiguously demonstrate that the elliptical enhancement occurs in an archetypal direct-gap semiconductor GaAs and is accompanied by the emergence of nonlinear optical activity, despite that GaAs hosts no magnetization or linear birefringence. Remarkably, the elliptical enhancement becomes pronounced only at particular intermediate excitation strengths. The excitation-strength dependence and polarization state of the harmonics indicate that interference among multiple nonlinear emission processes plays a key role. Such an interference of nonlinear processes can be controlled by changing the ellipticity of excitation field when the HHG occurs in the region of anisotropic band structure, and hence, elliptical enhancement occurs effectively in higher-order HHG. Further, microscopic calculations imply that such interfering nonlinear processes are rooted in the interband transitions among multiple bands of a solid (in the case of GaAs, transitions between the conduction and light-, heavy-, split-off hole bands). Our study reveals that, besides the material properties, an optimal-strength excitation that can be used to fine tune the nonlinear dynamics is especially important for controlling HHG properties, providing an alternative perspective for ultrafast light-control of solid-state materials.

DOI: [10.1103/PhysRevB.108.205201](https://doi.org/10.1103/PhysRevB.108.205201)**I. INTRODUCTION**

High harmonics (HHs) generated by irradiating a medium with intense laser pulses are a prominent example of extreme nonlinear optical phenomena [1]; they provide a platform to study the physics of ultrafast electron dynamics, and can be used as femtosecond and attosecond light sources. Recently, studies on HH generation (HHG) have been extended to solid-state materials [2–6], thanks to advances in pulse generation techniques in the midinfrared (MIR) and terahertz (THz) regions [7–11] that enable excitation of solids with an intense light field without damaging the sample. In solids, excited electrons are driven within the band structure, which is in stark contrast to the case of gases where the excited electrons run free in the vacuum. Under an intense light field, the excited electrons are driven in a wide range of the Brillouin zone, and the ultrafast dynamics taking place therein play a crucial role in HHG. Therefore, HHG in solids is expected to be a probe of dynamic material properties such as band structures [12–15], transition dipoles [16,17], and Berry curvatures [18–20].

Not only observing HH, but exploring the method to control HH properties is further important for the application of

HHG as a light source. It can also shed new light on the fundamental physics underlying HHG. For this purpose, there are several tunable parameters in the excitation light. In particular, besides the wavelength and pulse duration, the polarization state of the excitation light field (E_{exc}) is an important degree of freedom with which to control light-driven electron dynamics in matters [21–35]. Indeed, the sensitivity of HHG on the ellipticity of the excitation polarization (ε_{exc}) has been utilized to produce isolated attosecond extreme ultraviolet pulses [36–38], for example.

In the case of single-pulse excitation of isotropic atomic gases, the HH yields monotonically decrease as ε_{exc} increases [39,40]. This behavior is attributed to a reduction in the recombination rate of the photoemitted electrons and parent atoms, and it confirms the validity of the three-step model for HHG in a gaseous medium [41,42]. On the other hand, the change in ε_{exc} has a nontrivial impact on HHG in solids because the laser-driven electron dynamics are affected by the band structure of the materials, whose anisotropies reflect the symmetries of their crystal and electronic structures [30,43–45]. The most striking phenomenon is the *enhancement* in HH yields at a finite ε_{exc} . Recently, HH intensities in graphene [31] and in the surface state of topological insulator [46] have been shown to increase more when excited by elliptically-polarized E_{exc} (elliptical E_{exc}) than by linearly-polarized E_{exc} (linear E_{exc}), a phenomenon we refer to as “elliptical enhancement”. In those reports, the anomalous ε_{exc} dependence was regarded

*These authors contributed equally to this work.

†Corresponding author: sekiguchi@crc.u-tokyo.ac.jp‡Corresponding author: hirori@scl.kyoto-u.ac.jp§Corresponding author: kanemitsu@scl.kyoto-u.ac.jp

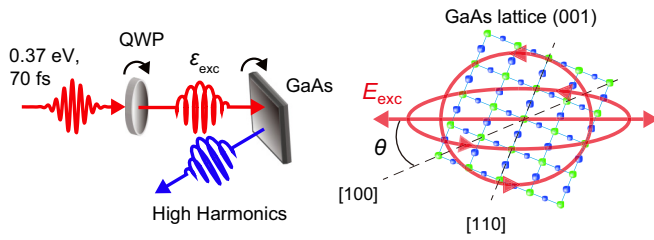


FIG. 1. Schematic image of high harmonics generation. The (001) surface of GaAs was irradiated with E_{exc} with a controlled ellipticity. θ denotes the angle between the major axis of E_{exc} polarization and the [100] crystal axis.

as a hallmark of the novel gapless state of the materials. However, the mechanism underlying the elliptical enhancement is still under discussion.

Meanwhile, it should be noted that several studies have reported a nonmonotonic dependence of HH intensities on ε_{exc} even in bulk materials with finite band gap energies; i.e., HH intensities show a peak at finite ε_{exc} [30,33]. Such a nonmonotonic ε_{exc} dependence was first explained with a real-space trajectory model in relation to the bond directions [30]. Later studies pointed out that the intraband and interband dynamics are affected differently by ε_{exc} , leading to a non-atom-like dependence on ε_{exc} [32,33]. Those reports, however, did not explicitly discuss the elliptical enhancement; it is not clear whether an elliptical E_{exc} can lead to a larger HH yield compared with the case of a linear E_{exc} applied along the most efficient crystal orientation for HHG.

Given this context, it remains elusive as to what materials, and under what excitation conditions, an elliptical enhancement can be obtained. Therefore, it is an urgent task to identify the key factor for the elliptical enhancement under well-controlled experimental conditions. To this end, we performed a systematic study of HHG in an archetypal direct-gap semiconductor GaAs. We measured the ε_{exc} dependence of HHG under various E_{exc} -field strengths and crystal orientations. We found that an elliptical enhancement does occur in GaAs at an *intermediate* E_{exc} -field strength in the nonperturbative excitation regime. The value of this optimal E_{exc} -field strength depends on the HH order. We also found that the elliptical enhancement is accompanied by nonlinear optical activity. We discuss how the elliptical enhancement occurs in GaAs on the basis of the experimental results of the E_{exc} -field dependence and polarization state of the generated HHs.

II. RESULTS

A. Experimental setup

Figure 1 shows a schematic image of the experimental setup. The (001) crystal surface of bulk GaAs was irradiated with 0.37-eV (3.4 μm in wavelength), 70-fs MIR pulses in almost normal incidence and with a tunable ellipticity of polarization, $\varepsilon_{\text{exc}} = E_{\text{min}}/E_{\text{max}}$, where E_{max} and E_{min} correspond to the field strength at the major and minor axes of the E_{exc} polarization ellipse. HHs were measured in the reflection geometry setup, where the wave-propagation effect inside the crystal can be minimized in the HHG process [47]. Odd-order HHs were observed up to the 13th order in the case of the

highest E_{exc} -field strength, ~ 10 MV/cm inside the sample crystal. In this paper, we focus on the HHs emitted above the band gap energy of 1.42 eV. While measuring the ε_{exc} dependence of the HH properties, the major axis direction of the elliptical E_{exc} polarization was fixed to a particular crystal orientation (see the Supplemental Material [48] for details). As shown in Fig. 1, θ is the angle between the major-axis direction of E_{exc} and the [100] crystal axis of GaAs.

B. Dependence of HH spectra on ε_{exc}

Figures 2(a) and 2(b) compare HH spectra generated by a linear ($\varepsilon_{\text{exc}} = 0$) and elliptical ($\varepsilon_{\text{exc}} = 0.3$) E_{exc} , measured at two different E_{exc} -field strengths. The crystal orientation was set at $\theta = 22.5^\circ$, which leads to the most efficient HHG by a strong linear E_{exc} (see Fig. 3 for the detailed θ dependence. The ε_{exc} dependence measured at $\theta = 0^\circ$ can be found in the Supplemental Material [48]). At the weak E_{exc} field of 4.8 MV/cm, the elliptical E_{exc} gives lower HH intensities compared with the linear E_{exc} . This behavior is commonly observed in atomic gases and has also been reported in solids [33,54–56].

On the other hand, the HH intensities show a highly non-trivial behavior under the strong E_{exc} field of 8.0 MV/cm. While the 5th- and 7th-order HH intensities become smaller in the case of an elliptical E_{exc} , the 9th- and 11th-order HH intensities become larger. The 13th-order HH intensity is almost the same for the linear and elliptical E_{exc} . These observations point out an important fact; the magnitude of the elliptical enhancement largely depends on the E_{exc} -field strength and HH order.

We confirmed this feature by measuring the ε_{exc} dependence of the HH intensities as shown in Figs. 2(c) and 2(d). Here, the HH intensities are normalized by the value for the linear E_{exc} ($\varepsilon_{\text{exc}} = 0$). Figure 2(c) shows the results for the 11th-order HH at different E_{exc} -field strengths. At lower E_{exc} fields, the HH intensity monotonically decreases as ε_{exc} increases, showing atom-like behavior. However, as the E_{exc} -field strength increases, the HH intensity starts to show a nonmonotonic ε_{exc} dependence with a peak structure, demonstrating that a strong E_{exc} field is necessary for an elliptical enhancement. The maximum HH yield is obtained around $\varepsilon_{\text{exc}} = 0.3$.

Furthermore, we found that HHs of different orders behave differently. Figure 2(d) shows the ε_{exc} dependence of the 7th-11th HH intensities generated with the E_{exc} field of 7.4 MV/cm. While the 9th- and 11th-order HHs show a peak around $\varepsilon_{\text{exc}} = 0.3$, the 7th-order HH decreases monotonically as ε_{exc} increases, in spite of the fact that they are generated by the same E_{exc} . To explain such a HH-order dependence, it is necessary to consider the emission process of each order individually.

While the major-axis direction of the E_{exc} polarization was fixed to a particular crystal orientation ($\theta = 22.5^\circ$) in Fig. 2, the θ dependence should also be carefully considered. Due to the anisotropy of the material, the HH yields change depending on θ even when the E_{exc} polarization is set to be linear ($\varepsilon_{\text{exc}} = 0$). This means that the normalization factor for the ε_{exc} dependence in Figs. 2(c) and 2(d) changes depending on θ . More importantly, as ε_{exc} increases, the E_{exc} -field

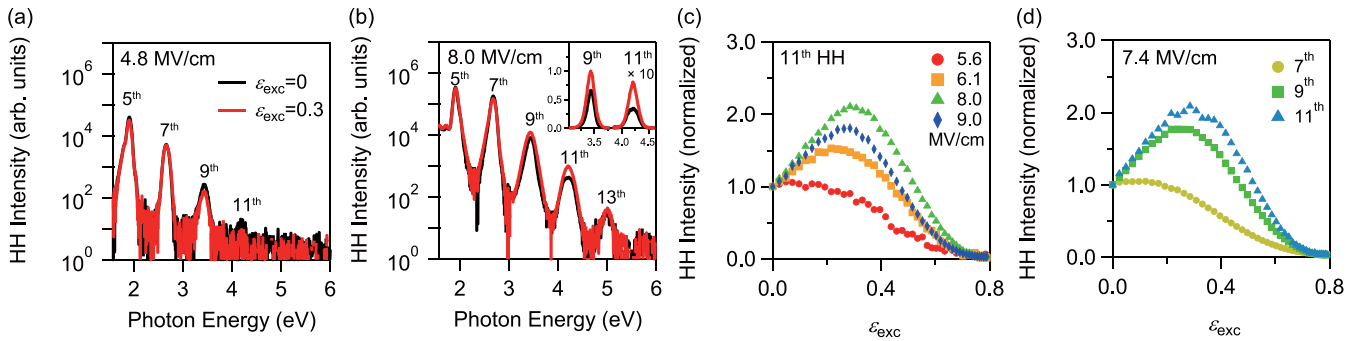


FIG. 2. (a), (b) HH spectra generated by linear ($\epsilon_{exc} = 0$) and elliptical ($\epsilon_{exc} = 0.3$) excitation, at E_{exc} -field strengths of (a) 4.8 MV/cm and (b) 8.0 MV/cm. (c) ϵ_{exc} dependence of 11th HH yield, normalized by the value at $\epsilon_{exc} = 0$, at different E_{exc} -field strengths. (d) ϵ_{exc} dependence of 7th, 9th and 11th HH yields at $E_{exc} = 7.4$ MV/cm, normalized by the value at $\epsilon_{exc} = 0$.

component perpendicular to the major-axis direction increases. If this perpendicular direction had a larger HHG efficiency compared with the major-axis direction, a scenario might possibly arise in which the elliptical enhancement is purely due to the yield anisotropy inherent to the material. To rule out this scenario, in the following we discuss the relation between the finite ellipticity of the E_{exc} -field polarization and the elliptical enhancement.

C. Unambiguous elliptical enhancement in GaAs

Figure 3 compares the θ dependences of the 9th- and 11th-HH intensities in the cases of linear ($\epsilon_{exc} = 0$) and elliptical ($\epsilon_{exc} = \pm 0.3$) excitations at different E_{exc} -field strengths. The depicted HH intensities at each field strength are normalized by the maximum value obtained by the linear E_{exc} . Notably, under the strong E_{exc} fields, the maximum HH intensity under the elliptical E_{exc} is obviously larger than that under the linear E_{exc} . In other words, the elliptical E_{exc} can generate a much larger HH intensity that can never be reached by the linear E_{exc} . This observation rules out the scenario in which the elliptical enhancement purely originates from the yield anisotropy,

and reveals that the finite ellipticity of the E_{exc} polarization is crucial.

Figure 3 unambiguously demonstrates that an elliptical enhancement of HHG occurs in GaAs, which is an archetypal semiconductor with a direct band gap of 1.42 eV. Therefore, the elliptical enhancement observed in this experiment is not related to the gapless states as had been proposed in the previous studies; rather, its essence lies in another mechanism. The experimental data show the importance of the phase control of the multiple emission processes contributing to a particular-order HHG, as we discuss step by step in the following.

D. Optimal field strength for elliptical enhancement

Figure 3 shows that the magnitude of the elliptical enhancement sensitively depends on the E_{exc} -field strength, as suggested in Fig. 2(c). At the lowest field of 4.1 MV/cm, the elliptical E_{exc} yields a smaller 9th-order HH intensity for any crystal orientation. The elliptical enhancement sets in as E_{exc} increases until it reaches a maximum at 5.6 MV/cm. However, further increase of E_{exc} suppresses the elliptical enhancement. This means that there exists an optimal field strength for the

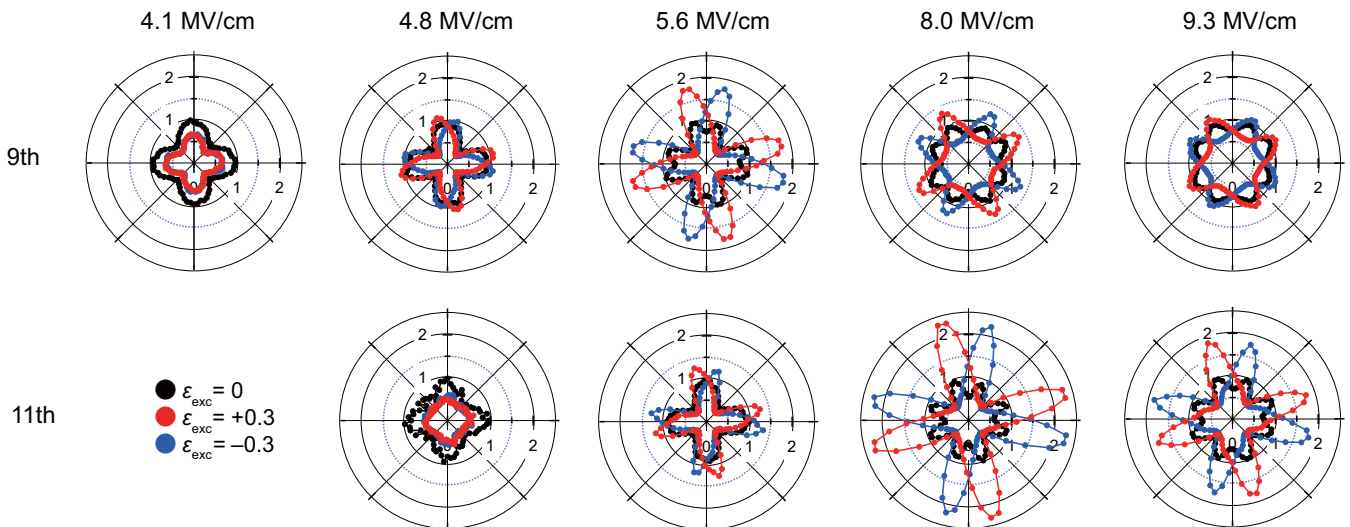


FIG. 3. θ dependence of the 9th and 11th HH yields at different E_{exc} -field strengths, generated by the linear ($\epsilon_{exc} = 0$) and elliptical ($\epsilon_{exc} = \pm 0.3$) E_{exc} . HH yields in each polar plot were normalized by the value of maximum HH yield obtained by linear E_{exc} at each field strength.

elliptical enhancement in the intermediate E_{exc} -field region. The same E_{exc} -field-strength dependence can be observed in the 11th HH. This behavior indicates that an extremely strong E_{exc} field does not guarantee an elliptical enhancement, but rather that some optimally tuned nonlinear dynamics is a key factor. Importantly, the optimal field strength for the elliptical enhancement depends on the HH order; ~ 5.6 MV/cm for the 9th HH and ~ 8.0 MV/cm for the 11th HH, as shown in Fig. 3. The difference in the optimal field depending on the HH order is not compatible with the interpretation based on the real-space crystal bond picture, which predicts that the largest HH yield is obtained for all orders of HH simultaneously when the electron trajectory matches a particular atomic-bond direction. Rather, the HH-order-dependent elliptical enhancement suggests that an “optimal tuning” of the nonlinear dynamics exists for each order of HHG individually.

E. Emergence of nonlinear optical activity

The elliptical enhancement in Fig. 3 is accompanied by another salient feature: elliptical dichroism. When the E_{exc} field is weak enough, the intensity of HH excited by the elliptical E_{exc} does not depend on the excitation helicity (the sign of ε_{exc}), and the linear and elliptical E_{exc} give a similar θ dependence, with the maximum being in the [100]-axis direction. However, as the field strength increases, the direction giving the maximum HH yield starts to deviate from the [100] axis. Notably, this deviation angle has opposite sign for the opposite excitation helicity. The magnitude of the elliptical dichroism, i.e., the contrast of the θ dependence relative to the opposite excitation helicity, reaches a maximum at the E_{exc} -field strength giving the largest elliptical enhancement. Therefore, it is reasonable to correlate the elliptical enhancement with the nonlinear elliptical dichroism. In addition, the apparent dependence on the sign of ε_{exc} confirms the crucial role of the phase difference between the E_{exc} -field components in the elliptical enhancement (for an example of decomposition, parallel (E_x) and perpendicular (E_y) components to the major axis of E_{exc}).

The emergence of elliptical dichroism in GaAs is counterintuitive, given the fact that bulk GaAs is nonmagnetic and does not show optical activity in the linear response. This observation indicates that GaAs excited by a strong E_{exc} field shows a chiral optical response in the nonlinear regime. Under such conditions, the polarization state of the HHs also show exotic behavior.

Figures 4(a) and 4(b) show the polarization state of the 11th HH generated by a linear and elliptical E_{exc} , respectively. Here, the crystal orientation is $\theta = 22.5^\circ$ and the field strength is 8.0 MV/cm, where the elliptical enhancement occurs in the 11th HH. Figure 4(a) shows that, under this excitation condition, the HH polarization becomes largely elliptical in spite of the linear polarization of E_{exc} . Hence, not only does elliptical dichroism appear as shown in Fig. 3, but also a polarization rotation does occur in HHG, revealing the emergence of nonlinear optical activity (NOA) in GaAs. Here, the fact that NOA appears under a linear E_{exc} field indicates that NOA does not require E_{exc} to have a finite ellipticity, and it originates from the strong- E_{exc} -field-driven electron dynamics in GaAs. We note that in high-order sideband

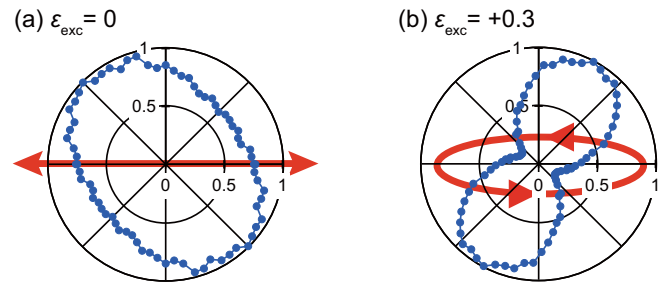


FIG. 4. (a), (b) Polarization state of the 11th HH generated by (a) linear ($\varepsilon_{\text{exc}} = 0$) and (b) elliptical ($\varepsilon_{\text{exc}} = +0.3$) excitation. $\theta = 22.5^\circ$ and $E_{\text{exc}} = 8.0$ MV/cm. The arrows depict the E_{exc} field.

generation, which is another nonperturbative nonlinear optical phenomenon induced by pulses with two different frequencies of near-infrared and THz, a related behavior “dynamical birefringence” was observed by using a linear THz E_{exc} field [20].

From a phenomenological point of view, NOA means that a nonlinear polarization perpendicular to the E_{exc} field is induced, indicating that cross terms in the relation between nonlinear polarization components (P_x and P_y) and E_{exc} components (E_x and E_y) appear under a strong E_{exc} field. Such a cross term is substantialized by off-diagonal nonlinear susceptibilities, which mixes E_x and E_y for generating HHs. This off-diagonal nonlinear response can be attributed to electron dynamics in the high energy region of the Brillouin zone away from the band edge in GaAs, whose structure has a sizable anisotropy. This picture based on the band anisotropy qualitatively explains the θ dependence of the elliptical dichroism in Fig. 3. The HH intensities by $\varepsilon_{\text{exc}} = \pm 0.3$ degenerate along $\theta = 0^\circ$ and 45° where the off-diagonal response is forbidden by the high symmetry of the band structure, while their contrast becomes sizable at low-symmetric crystal orientation (around $\theta = 22.5^\circ$). The actual band structure of GaAs is shown later in Fig. 7.

Let us discuss Fig. 4 in more detail. The large ellipticity of the 11th HH indicates that there are multiple emission processes with different polarization directions and temporal phases, and they contribute to the HHG at the same energy. On the other hand, the HH ellipticity becomes smaller in the case of an elliptical E_{exc} , as shown in Fig. 4(b). It is counterintuitive that an increase in ε_{exc} results in a decrease in the ellipticity of the generated HH. The decrease in HH ellipticity indicates that the above-mentioned phase difference in the emission processes can be compensated by using an elliptical E_{exc} . Therefore, the comparison of Figs. 4(a) and 4(b) demonstrates that it is possible to control the phase difference of the nonlinear polarizations leading to HHG by changing ε_{exc} . This phase control of HHG is mediated by the aforementioned off-diagonal response, through which ε_{exc} , i.e., the phase difference between E_x and E_y , can exert an influence on the nonlinear polarizations.

F. Dependence of magnitude of elliptical enhancement on E_{exc} -field strength

Next, we discuss the relation between the multiple nonlinear processes underlying NOA and the elliptical enhancement of HHG, by analyzing the E_{exc} -field-strength dependence of

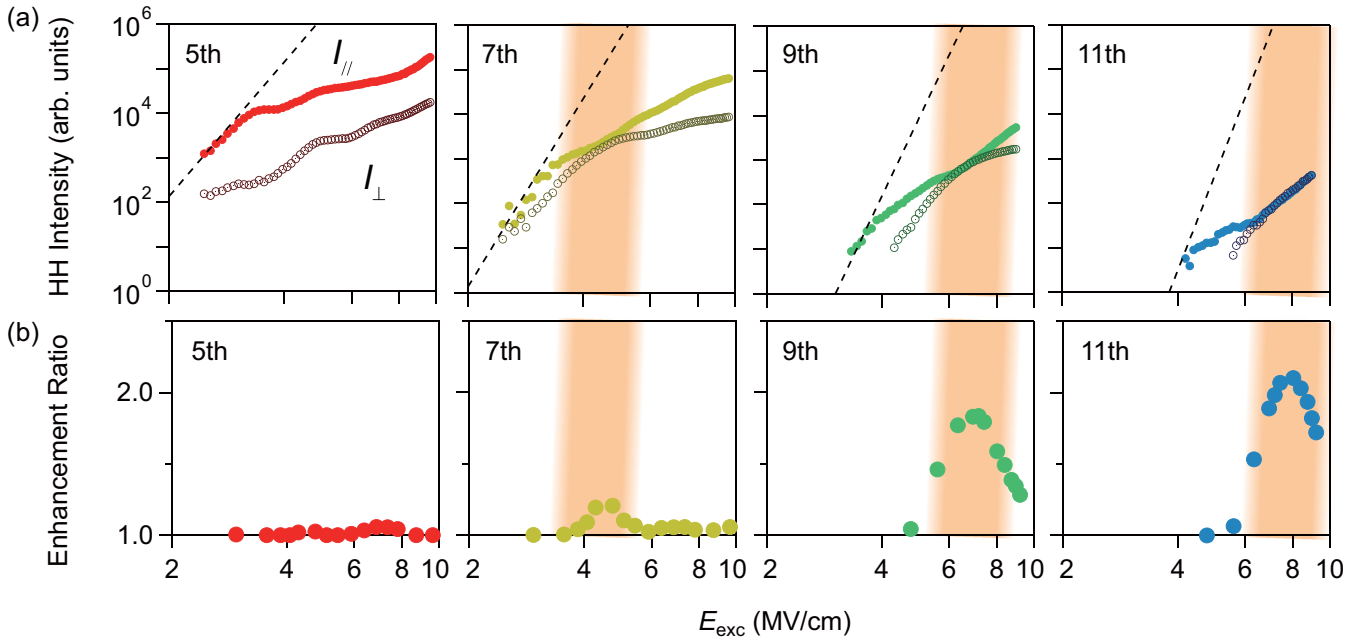


FIG. 5. (a) E_{exc} -field-strength dependence of I_{\parallel} and I_{\perp} of 5th-11th HHs, generated by a linear E_{exc} at $\theta = 22.5^\circ$. (b) E_{exc} -field-strength dependence of the magnitude of elliptical enhancement at $\theta = 22.5^\circ$.

the HH intensities. Figure 5(a) plots the intensities of the 5th-11th HHs generated by the linear E_{exc} at $\theta = 22.5^\circ$, where the polarization components parallel (I_{\parallel}) or perpendicular (I_{\perp}) to E_{exc} are resolved. As the field strength increases, the HH intensities deviate from the perturbative power-law scaling, indicating that nonperturbative HHG occurs in a stronger E_{exc} field. In the HHs of all orders, I_{\parallel} and I_{\perp} show distinctly different dependences on the E_{exc} -field strength. This fact indicates that the I_{\parallel} and I_{\perp} are not expressible as simple projections of a single HH emission source in each direction. Instead, it suggests the existence of multiple emission processes contributing to HH of a particular order. These emission processes have different E_{exc} -field-strength dependence (in other words, the order of nonlinearity), in addition to different polarization directions.

The curves of I_{\parallel} and I_{\perp} in Fig. 5(a) have several kinks in the nonperturbative region. In particular, I_{\parallel} and I_{\perp} of the 7th-11th HHs show a pronounced kink in the intermediate E_{exc} region, where the contribution of I_{\parallel} and I_{\perp} become comparable. Upon crossing the kink, the derivatives of I_{\parallel} and I_{\perp} changes, i.e., the nonlinear order of the HHG process changes. Therefore, the kinks can be regarded as a switching of the dominant contribution from one nonlinear process to another. As a result, the contributions from several nonlinear processes to HHG become comparable, and they interfere, around the kinks in I_{\parallel} and I_{\perp} in the intermediate E_{exc} region [45].

Notably, a pronounced elliptical enhancement occurs around the E_{exc} -field strength leading to the kink of I_{\parallel} and I_{\perp} . The magnitude of the elliptical enhancement is plotted as a function of the E_{exc} -field strength in Fig. 5(b) (see also Supplemental Material [48] for the complete data set). Here, the magnitude was determined from the maximum value of the ε_{exc} -dependent HH yield, as shown in Figs. 2(c) and 2(d). Figure 5(b) reconfirms that the elliptical enhancement reaches a maximum at an optimal E_{exc} field depending on the HH

order. This optimal field strength coincides with the region around the kink in the plots of Fig. 5(b).

Therefore, an elliptical enhancement can be realized in the intermediate E_{exc} -field region where multiple nonlinear processes give comparable contributions to HH of a particular order. This observation suggests a possible mechanism behind the elliptical enhancement. As can be seen in Fig. 4, by changing ε_{exc} , one can control the phase difference among the nonlinear emission processes. When this leads to suppression of destructive interference among the emission processes, the HH yield is enhanced.

III. DISCUSSION

Now we schematically show how the above-mentioned mechanism works; we use a phenomenological picture describing how the control of the phase difference among the nonlinear emission processes can result in an enhancement of the HH yield.

For simplicity, let us assume there are two nonlinear processes contributing to a particular order of HH. They have different emission phases and E_{exc} -field-strength dependences:

$$\begin{aligned} I_{HH} \propto |\bar{P}_{HH}|^2 &= |\bar{A}(\vec{E}_{\text{exc}})e^{i\varphi_1} + \bar{B}(\vec{E}_{\text{exc}})e^{i\varphi_2}|^2 \\ &= |\bar{A}(\vec{E}_{\text{exc}}) + \bar{B}(\vec{E}_{\text{exc}})e^{i(\varphi_1 - \varphi_2)}|^2. \end{aligned} \quad (1)$$

In a simple case, these two different terms might correspond to the different-order nonlinear processes, such as n th and $(n+2)$ th, where n is an integer, contributing to emission at the energy of n th HHG [6,45]. This assumption is based on the lowest-order approximation valid at the entrance to the crossover between the perturbative and non-perturbative nonlinear regime [45], and hence, it becomes less realistic in the deeply nonperturbative nonlinear region under

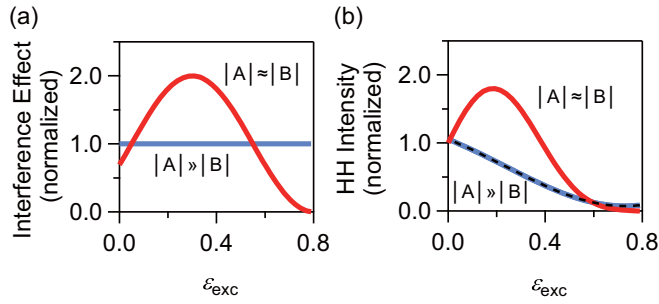


FIG. 6. (a) Schematic plot of ε_{exc} dependence of the interference effect. (b) Black dashed line: atom-like ε_{exc} dependence of HH yield, which appears in the low- E_{exc} -field perturbative regime. Solid lines: ε_{exc} dependence of the HH intensities, obtained by multiplying the solid lines in (a) by the dashed line in (b).

the extremely-strong E_{exc} . The result of numerical simulation, which complements the phenomenological model, will be shown later. If the two terms have similar polarization directions, we can approximate Eq. (1) as

$$I_{HH} \sim |A(E_{\text{exc}})|^2 + |B(E_{\text{exc}})|^2 + 2|A(E_{\text{exc}})||B(E_{\text{exc}})| \cos(\varphi_1 - \varphi_2) \quad (2)$$

The effect of the phase difference $\varphi_1 - \varphi_2$ should be negligible in the case that $|A(E_{\text{exc}})| \gg |B(E_{\text{exc}})|$ or $|A(E_{\text{exc}})| \ll |B(E_{\text{exc}})|$, where the HHG is dominated by a single nonlinear process, $I_{HH} \sim |A(E_{\text{exc}})|^2$ or $I_{HH} \sim |B(E_{\text{exc}})|^2$. On the other hand, phase difference affects the HH intensity when the contributions from the two terms are comparable, i.e., $|A(E_{\text{exc}})| \approx |B(E_{\text{exc}})|$.

To illustrate the proposed mechanism of the elliptical enhancement, we will assume that the phase difference $\varphi_1 - \varphi_2$ can be monotonically tuned by changing ε_{exc} . The ability of such a phase control by ε_{exc} is related to the band structure of the material, as discussed later. The solid curves in Fig. 6(a) show how the HH yield depends on ε_{exc} in the case of $|A(E_{\text{exc}})| \gg |B(E_{\text{exc}})|$ and $|A(E_{\text{exc}})| \approx |B(E_{\text{exc}})|$, with only considering the interference between the nonlinear processes. Here, it should be noted that even in the low E_{exc} -field region, the HH yields show the monotonic ε_{exc} dependence of atom-like behavior, as shown in Fig. 2(c) for example, which can be attributed to suppression of the carrier excitation and recombination rate. To incorporate this feature, we multiply the solid lines in Fig. 6(a) by the monotonically decreasing dashed line in Fig. 6(b), which qualitatively reproduces the atom-like ε_{exc} dependence at low E_{exc} fields. The resultant dependence of the HH yield on ε_{exc} are shown as the solid lines in Fig. 6(b). The lines in the case of $|A(E_{\text{exc}})| \gg |B(E_{\text{exc}})|$ and $|A(E_{\text{exc}})| \approx |B(E_{\text{exc}})|$ qualitatively reproduce the ε_{exc} dependence where an enhancement does and does not occur, respectively.

The model described above enabled us to understand how the control of the phases of nonlinear processes by changing ε_{exc} can potentially induce an elliptical enhancement, and it qualitatively explains the E_{exc} -field-strength dependence. On the other hand, there is another key factor for realizing elliptical enhancement, that is, the HH order. As can be seen in Fig. 5(b), the elliptical enhancement becomes more pronounced in higher-order HHs. In other words, the elliptical

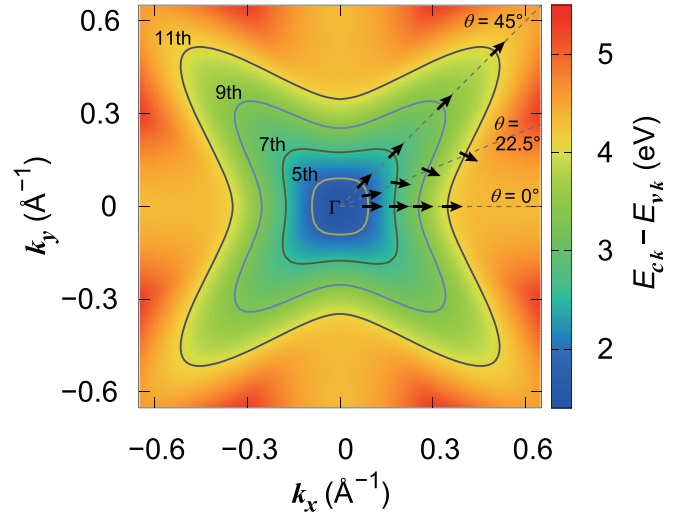


FIG. 7. Two-dimensional map of the energy difference between the conduction band bottom and the valence band top of GaAs with (001) surface. The k_x and k_y axes correspond to the Γ -X direction. The solid lines represent the interband transition energies for HHG of each order. The arrows represent the direction of the gradient of the energy surface at representative k points along several directions, corresponding to the real-space crystal orientation of $\theta = 0^\circ$, 22.5° , and 45° .

enhancement becomes less significant in lower-order HHs. This can be attributed to the fact that the lower-order HHs have energies close to the band gap of GaAs. Figure 7 shows a color map of the interband transition energy between the highest valence band and lowest conduction band, $E_{ck} - E_{vk}$, derived from the calculated band structure of GaAs with a (001) crystal surface [51]. The orientations of k_x and k_y correspond to the Γ -X direction, i.e., the [100] crystal orientation. The solid lines correspond to the interband transition energies for HHG of each order, and the arrows represent the direction of the gradient of energy surface at representative k points. As can be seen in Fig. 7, the 5th HH is emitted from the k points close to the band center (Γ point), where the band landscape is almost isotropic. Therefore, the 5th HH shows an atom-like behavior, and hence, the elliptical enhancement does not occur effectively. On the other hand, higher-order HHs with larger emission energies are generated at k points away from the band center, where the anisotropy of the band landscape becomes more and more significant. In particular, the warping of the energy surface appears along the low symmetric crystal orientation, as the directions of gradient at k points along the $\theta = 22.5^\circ$ orientation deviate from the radial axis. This anisotropic band structure leads to an effective off-diagonal nonlinear response, that mixes E_x and E_y for generating HHs. Owing to this feature, the change of ε_{exc} , i.e., the phase difference between E_x and E_y , can exert influence on the phases of nonlinear polarizations φ_1 and φ_2 in Eq. (1). Since the two terms in Eq. (1) have different nonlinear order, the influence of ε_{exc} on the phase difference $\varphi_1 - \varphi_2$ survives in Eq. (2), and hence, $\varphi_1 - \varphi_2$ can be tuned by ε_{exc} enabling an elliptical enhancement under a suitable E_{exc} -field strength. Therefore, an elliptical enhancement requires interplay between two features, i.e., well-controlled interfer-

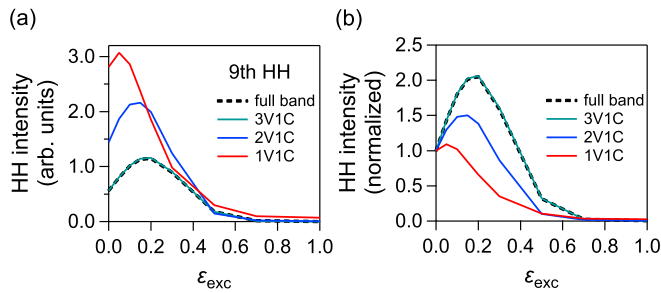


FIG. 8. Calculated ε_{exc} dependence of the intensity of the 9th HH. $\theta = 22.5^\circ$ and $E_{\text{exc}} = 8.0 \text{ MV/cm}$. (a) Raw HH intensity. (b) HH intensity normalized by the value at $\varepsilon_{\text{exc}} = 0$. Note that the full band calculation actually corresponds to the 4V1C band calculation.

ence of multiple nonlinear processes and an anisotropic band structure where the HH emission occurs. The former feature in turn requires a fine-tuned E_{exc} strength, while the latter requires the emission energy to be far from the band edge. This leads to the elliptical enhancement effective for higher order HH at an intermediate E_{exc} -field strength, as revealed in Fig. 5(b).

Finally, we discuss about the microscopic origin of the interfering multiple nonlinear processes; we assumed that different-order and different-phase nonlinear processes contribute to a particular-order HH in the phenomenological picture, but how are those processes related to the material property of GaAs? Several reports suggested the important role of interference of interband transitions between different pairs of the bands played in the nonperturbative nonlinear optical phenomena [20,57], which can be relevant to the proposed picture in this study. To clarify this point, we theoretically calculate the HH intensity based on the band structure of GaAs. We compare the ε_{exc} dependences of the HH intensity calculated with including different numbers of the bands, i.e., full band set v.s. limited band set (see Supplemental Material [48] for details of the simulation). Under the excitation condition of $E_{\text{exc}} = 8.0 \text{ MV/cm}$ and $\theta = 22.5^\circ$, the calculated 9th HH shows elliptical enhancement as shown in Fig. 8. Figure 8(a) compares the intensity of the 9th HH calculated with involving full bands or limited numbers of bands. Here, 1,2,3 valence (V) bands and 1 conduction (C) band are considered, which corresponds to the light-, heavy- and split-off hole bands and the first conduction band. The calculation with including full bands and 3V1C bands give almost the same HH intensity, indicating that the interband transitions between the three highest valence bands and the one lowest conduction band dominate the generation of 9th HH. On the other hand, further reduction of the number of the bands (2V1C and 1V1C case) leads to an enhancement of the HH intensity. It is noteworthy that inclusion of the least number of bands (the two-band model of 1V1C) results in the largest HH intensity. This behavior indicates that the destructive interference among the interband transitions between the conduction and the multiple valence bands leads to the suppression of the HH intensity. Figure 8(b) shows the ε_{exc} dependences of the HH intensity normalized by the value for the linear $E_{\text{exc}}(\varepsilon_{\text{exc}} = 0)$. Here, the elliptical enhancement (enhancement of ~ 2) clearly

occurs in full- and 3V1C-bands calculation. However, the enhancement becomes smaller in 2V1C-bands case, and can be hardly discerned in 1V1C-bands case. Combined with the result in Fig. 8(a), the elliptical enhancement becomes substantial when the destructive interference among the interband transitions has a significant influence on the HH intensity. This is consistent with the phenomenological picture that the elliptical enhancement occurs when a destructive interference between nonlinear emission processes gets suppressed by the elliptical E_{exc} . Figure 8(b) shows that the number of valence bands involved in the HHG process has a significant impact on the magnitude of the elliptical enhancement. Therefore, the interfering multiple nonlinear processes in the phenomenological picture can be largely rooted in the interband transitions among multiple bands of a solid, which can have different nonlinear orders and phases.

For a further careful discussion, we also mention that, in Fig. 8, a tiny enhancement appears at small ε_{exc} even in the 1V1C-band calculation. In general, nonlinear processes with different nonlinear orders and phases can arise due to the different electron trajectories, and the interplay between intraband and interband transitions, even in a two-band model. Hence, the interference between such different nonlinear processes can lead to a finite elliptical enhancement in a two-band material, while Fig. 8 shows that its magnitude can be boosted by the multiband nature.

To summarize, we investigated the dependence of HHG on ε_{exc} in GaAs at various E_{exc} -field strengths and crystal orientations. We unambiguously demonstrated that elliptical enhancement occurs in GaAs. This enhancement does not stem solely from the anisotropic HH yield inherent to the crystal; the finite ellipticity of E_{exc} polarization plays a crucial role. The elliptical enhancement is accompanied by the emergence of nonlinear optical activity. Importantly, both the elliptical enhancement and nonlinear optical activity become pronounced at an intermediate optimal E_{exc} -field strength. This E_{exc} -field dependence and polarization state of the HHs indicate that the elliptical enhancement is an outcome of the controlled interference effect of multiple HH emission processes, which is enabled by the anisotropic band structure and is therefore effective for higher-order HHG. Microscopic calculations imply that such interfering HH emission processes originate from the interband transitions among multiple bands of a solid. Our experimental and theoretical results will stimulate not only studies to further uncover the microscopic electron dynamics that relates characteristic HHG in solids with the detail of material properties, but also explorations of novel nonlinear phenomena in a wide range of solid-state materials. Our study provides an alternative perspective for efficient control of light-driven ultrafast phenomena in solids.

ACKNOWLEDGMENTS

Part of this study was supported by a grant from the Japan Society for the Promotion of Science (JPSP KANENHI Grant No. JP19H05465). Computational resource of Fujitsu PRIMEHPC FX1000 and FUJITSU PRIMERGY GX2570 (Wisteria/BDEC-01) was awarded by ‘‘Multidisciplinary Cooperative Research Program (MCRP) 2023’’, Center for Computational Sciences, University of Tsukuba.

- [1] P. B. Corkum and F. Krausz, Attosecond science, *Nat. Phys.* **3**, 381 (2007).
- [2] A. H. Chin, O. G. Calderón, and J. Kono, Extreme midinfrared nonlinear optics in semiconductors, *Phys. Rev. Lett.* **86**, 3292 (2001).
- [3] S. Ghimire, A. D. DiChiara, E. Sistrunk, P. Agostini, L. F. DiMauro, and D. A. Reis, Observation of high-order harmonic generation in a bulk crystal, *Nat. Phys.* **7**, 138 (2011).
- [4] D. Golde, T. Meier, and S. W. Koch, High harmonics generated in semiconductor nanostructures by the coupled dynamics of optical inter- and intraband excitations, *Phys. Rev. B* **77**, 075330 (2008).
- [5] G. Vampa, C. R. McDonald, G. Orlando, D. D. Klug, P. B. Corkum, and T. Brabec, Theoretical analysis of high-harmonic generation in solids, *Phys. Rev. Lett.* **113**, 073901 (2014).
- [6] K. Nakagawa, H. Hirori, S. A. Sato, H. Tahara, F. Sekiguchi, G. Yumoto, M. Saruyama, R. Sato, T. Teranishi, and Y. Kanemitsu, Size-controlled quantum dots reveal the impact of intraband transitions on high-order harmonic generation in solids, *Nat. Phys.* **18**, 874 (2022).
- [7] A. Sell, A. Leitenstorfer, and R. Huber, Phase-locked generation and field-resolved detection of widely tunable terahertz pulses with amplitudes exceeding 100 MV/cm, *Opt. Lett.* **33**, 2767 (2008).
- [8] H. Hirori, A. Doi, F. Blanchard, and K. Tanaka, Single-cycle terahertz pulses with amplitudes exceeding 1 MV/cm generated by optical rectification in LiNbO₃, *Appl. Phys. Lett.* **98**, 91106 (2011).
- [9] G. Andriukaitis, T. Balčiūnas, S. Ališauskas, A. Pugžlys, A. Baltuška, T. Popmintchev, M.-C. Chen, M. M. Murnane, and H. C. Kapteyn, 90 GW peak power few-cycle midinfrared pulses from an optical parametric amplifier, *Opt. Lett.* **36**, 2755 (2011).
- [10] N. Kanda, N. Ishii, J. Itatani, and R. Matsunaga, Optical parametric amplification of phase-stable terahertz-to-midinfrared pulses studied in the time domain, *Opt. Express* **29**, 3479 (2021).
- [11] Y. Sanari, F. Sekiguchi, K. Nakagawa, N. Ishii, Y. Kanemitsu, and H. Hirori, Generation of wavelength-tunable few-cycle pulses in the midinfrared at repetition rates up to 10 kHz, *Opt. Lett.* **46**, 5280 (2021).
- [12] T. T. Luu, M. Garg, S. Y. Kruchinin, A. Moulet, M. T. Hassan, and E. Goulielmakis, Extreme ultraviolet high-harmonic spectroscopy of solids, *Nature (London)* **521**, 498 (2015).
- [13] G. Vampa, T. J. Hammond, N. Thiré, B. E. Schmidt, F. Légaré, C. R. McDonald, T. Brabec, D. D. Klug, and P. B. Corkum, All-optical reconstruction of crystal band structure, *Phys. Rev. Lett.* **115**, 193603 (2015).
- [14] A. J. Uzan, G. Orenstein, Á. Jiménez-Galán, C. McDonald, R. E. F. Silva, B. D. Bruner, N. D. Klimkin, V. Blanchet, T. Arusi-Parpar, M. Krüger, A. N. Rubtsov, O. Smirnova, M. Ivanov, B. Yan, T. Brabec, and N. Dudovich, Attosecond spectral singularities in solid-state high-harmonic generation, *Nat. Photonics* **14**, 183 (2020).
- [15] A. J. Uzan-Narovlansky, Á. Jiménez-Galán, G. Orenstein, R. E. F. Silva, T. Arusi-Parpar, S. Shames, B. D. Bruner, B. Yan, O. Smirnova, M. Ivanov, and N. Dudovich, Observation of light-driven band structure via multiband high-harmonic spectroscopy, *Nat. Photonics* **16**, 428 (2022).
- [16] S. Jiang, J. Chen, H. Wei, C. Yu, R. Lu, and C. D. Lin, Role of the transition dipole amplitude and phase on the generation of odd and even high-order harmonics in crystals, *Phys. Rev. Lett.* **120**, 253201 (2018).
- [17] K. Uchida, V. Pareek, K. Nagai, K. M. Dani, and K. Tanaka, Visualization of two-dimensional transition dipole moment texture in momentum space using high-harmonic generation spectroscopy, *Phys. Rev. B* **103**, L161406 (2021).
- [18] H. Liu, Y. Li, Y. S. You, S. Ghimire, T. F. Heinz, and D. A. Reis, High-harmonic generation from an atomically thin semiconductor, *Nat. Phys.* **13**, 262 (2017).
- [19] T. T. Luu and H. J. Wörner, Measurement of the Berry curvature of solids using high-harmonic spectroscopy, *Nat. Commun.* **9**, 916 (2018).
- [20] H. B. Banks, Q. Wu, D. C. Valocin, S. Mack, A. C. Gossard, L. Pfeiffer, R.-B. Liu, and M. S. Sherwin, Dynamical birefringence: electron-hole recollisions as probes of berry curvature, *Phys. Rev. X*, **7** 041042 (2017).
- [21] T. Oka and H. Aoki, Photovoltaic Hall effect in graphene, *Phys. Rev. B* **79**, 081406 (2009).
- [22] J. W. McIver, B. Schulte, F.-U. Stein, T. Matsuyama, G. Jotzu, G. Meier, and A. Cavalleri, Light-induced anomalous Hall effect in graphene, *Nat. Phys.* **16**, 38 (2020).
- [23] E. J. Sie, J. W. McIver, Y.-H. Lee, L. Fu, J. Kong, and N. Gedik, Valley-selective optical Stark effect in monolayer WS₂, *Nat. Mater.* **14**, 290 (2015).
- [24] T. Higuchi, C. Heide, K. Ullmann, H. B. Weber, and P. Hommelhoff, Light-field-driven currents in graphene, *Nature (London)* **550**, 224 (2017).
- [25] G. Yumoto, H. Hirori, F. Sekiguchi, R. Sato, M. Saruyama, T. Teranishi, and Y. Kanemitsu, Strong spin-orbit coupling inducing Autler-Townes effect in lead halide perovskite nanocrystals, *Nat. Commun.* **12**, 3026 (2021).
- [26] I. J. Kim, C. M. Kim, H. T. Kim, G. H. Lee, Y. S. Lee, J. Y. Park, D. J. Cho, and C. H. Nam, Highly efficient high-harmonic generation in an orthogonally polarized two-color laser field, *Phys. Rev. Lett.* **94**, 243901 (2005).
- [27] D. Shafir, H. Soifer, B. D. Bruner, M. Dagan, Y. Mairesse, S. Patchkovskii, M. Y. Ivanov, O. Smirnova, and N. Dudovich, Resolving the time when an electron exits a tunnelling barrier, *Nature (London)* **485**, 343 (2012).
- [28] O. Kfir, P. Grychtol, E. Turgut, R. Knut, D. Zusin, D. Popmintchev, T. Popmintchev, H. Nembach, J. M. Shaw, A. Fleischer, H. Kapteyn, M. Murnane, and O. Cohen, Generation of bright phase-matched circularly-polarized extreme ultraviolet high harmonics, *Nat. Photonics* **9**, 99 (2015).
- [29] O. Neufeld and O. Cohen, Optical chirality in nonlinear optics: application to high harmonic generation, *Phys. Rev. Lett.* **120**, 133206 (2018).
- [30] Y. S. You, D. A. Reis, and S. Ghimire, Anisotropic high-harmonic generation in bulk crystals, *Nat. Phys.* **13**, 345 (2017).
- [31] N. Yoshikawa, T. Tamaya, and K. Tanaka, High-harmonic generation in graphene enhanced by elliptically polarized light excitation, *Science* **356**, 736 (2017).
- [32] N. Tancogne-Dejean, O. D. Mücke, F. X. Kärtner, and A. Rubio, Ellipticity dependence of high-harmonic generation in solids originating from coupled intraband and interband dynamics, *Nat. Commun.* **8**, 745 (2017).
- [33] N. Klemke, N. Tancogne-Dejean, G. M. Rossi, Y. Yang, F. Scheiba, R. E. Mainz, G. Di Sciaccia, A. Rubio, F. X. Kärtner, and O. D. Mücke, Polarization-state-resolved high-harmonic spectroscopy of solids, *Nat. Commun.* **10**, 1319 (2019).

- [34] X. Zhang, J. Li, Z. Zhou, S. Yue, H. Du, L. Fu, and H.-G. Luo, Ellipticity dependence transition induced by dynamical Bloch oscillations, *Phys. Rev. B* **99**, 014304 (2019).
- [35] Y. Sanari, T. Otake, Y. Kanemitsu, and H. Hirori, Modifying angular and polarization selection rules of high-order harmonics by controlling electron trajectories in k-space, *Nat. Commun.* **11**, 3069 (2020).
- [36] G. Sansone, E. Benedetti, F. Calegari, C. Vozzi, L. Avaldi, R. Flammini, L. Poletto, P. Villoresi, C. Altucci, R. Velotta, S. Stagira, S. De Silvestri, and M. Nisoli, Isolated single-cycle attosecond pulses., *Science* **314**, 443 (2006).
- [37] H. Mashiko, S. Gilbertson, C. Li, S. D. Khan, M. M. Shakya, E. Moon, and Z. Chang, Double optical gating of high-order harmonic generation with carrier-envelope phase stabilized lasers, *Phys. Rev. Lett.* **100**, 103906 (2008).
- [38] J. Li, X. Ren, Y. Yin, K. Zhao, A. Chew, Y. Cheng, E. Cunningham, Y. Wang, S. Hu, Y. Wu, M. Chini, and Z. Chang, 53-attosecond X-ray pulses reach the carbon K-edge, *Nat. Commun.* **8**, 186 (2017).
- [39] K. S. Budil, P. Salières, A. L’Huillier, T. Ditmire, and M. D. Perry, Influence of ellipticity on harmonic generation, *Phys. Rev. A* **48**, R3437 (1993).
- [40] P. Dietrich, N. H. Burnett, M. Ivanov, and P. B. Corkum, High-harmonic generation and correlated two-electron multiphoton ionization with elliptically polarized light, *Phys. Rev. A* **50**, R3585 (1994).
- [41] P. B. Corkum, Plasma perspective on strong field multiphoton ionization, *Phys. Rev. Lett.* **71**, 1994 (1993).
- [42] M. Lewenstein, P. Balcou, M. Y. Ivanov, A. L’Huillier, and P. B. Corkum, Theory of high-harmonic generation by low-frequency laser fields, *Phys. Rev. A* **49**, 2117 (1994).
- [43] F. Langer, M. Hohenleutner, U. Huttner, S. W. Koch, M. Kira, and R. Huber, Symmetry-controlled temporal structure of high-harmonic carrier fields from a bulk crystal, *Nat. Photonics* **11**, 227 (2017).
- [44] K. Kaneshima, Y. Shinohara, K. Takeuchi, N. Ishii, K. Imasaka, T. Kaji, S. Ashihara, K. L. Ishikawa, and J. Itatani, Polarization-resolved study of high harmonics from bulk semiconductors, *Phys. Rev. Lett.* **120**, 243903 (2018).
- [45] F. Sekiguchi, G. Yumoto, H. Hirori, and Y. Kanemitsu, Polarization anomaly in high harmonics in the crossover region between perturbative and extreme nonlinearity in GaAs, *Phys. Rev. B* **106**, L241201 (2022).
- [46] C. Heide, Y. Kobayashi, D. R. Baykusheva, D. Jain, J. A. Sobota, M. Hashimoto, P. S. Kirchmann, S. Oh, T. F. Heinz, D. A. Reis, and S. Ghimire, Probing topological phase transitions using high-harmonic generation, *Nat. Photonics* **16**, 620 (2022).
- [47] P. Xia, C. Kim, F. Lu, T. Kanai, H. Akiyama, J. Itatani, and N. Ishii, Nonlinear propagation effects in high harmonic generation in reflection and transmission from gallium arsenide, *Opt. Express* **26**, 29393 (2018).
- [48] See Supplemental Material at <http://link.aps.org/supplemental/10.1103/PhysRevB.108.205201> for the details of experimental setup, the dependence of HH intensities measured at different values of θ , complete dataset for the magnitude of elliptical enhancement, and the description of the simulation of microscopic electron dynamics, which includes Refs. [49–53].
- [49] S. A. Sato, J. W. McIver, M. Nuske, P. Tang, G. Jotzu, B. Schulte, H. Hübener, U. De Giovannini, L. Mathey, M. A. Sentef, A. Cavalleri, and A. Rubio, Microscopic theory for the light-induced anomalous Hall effect in graphene, *Phys. Rev. B* **99**, 214302 (2019).
- [50] Wenwen Mao, Angel Rubio, and Shunsuke A. Sato, Terahertz-induced high-order harmonic generation and nonlinear charge transport in graphene, *Phys. Rev. B* **106**, 024313 (2022).
- [51] Y. Tan, M. Povolotskiy, T. Kubis, Y. He, Z. Jiang, G. Klimeck, and T. B. Boykin, Empirical tight binding parameters for GaAs and MgO with explicit basis through DFT mapping, *J. Comput. Electron.* **12**, 56 (2013).
- [52] P. Vogl, Harold P. Hjalmarson, and John D. Dow, A Semi-empirical tight-binding theory of the electronic structure of semiconductors, *J. Phys. Chem. Solids* **44**, 365 (1983).
- [53] J.-M. Jancu, R. Scholz, F. Beltram, and F. Bassani, Empirical sp³* tight-binding calculation for cubic semiconductors: General method and material parameters, *Phys. Rev. B* **57**, 6493 (1998).
- [54] K. Nakagawa, H. Hirori, Y. Sanari, F. Sekiguchi, R. Sato, M. Saruyama, T. Teranishi, and Y. Kanemitsu, Interference effects in high-order harmonics from colloidal perovskite nanocrystals excited by an elliptically polarized laser, *Phys. Rev. Mater.* **5**, 016001 (2021).
- [55] C. Liu, Y. Zheng, Z. Zeng, and R. Li, Effect of elliptical polarization of driving field on high-order-harmonic generation in semiconductor ZnO, *Phys. Rev. A* **93**, 043806 (2016).
- [56] G. Ndabashimiye, S. Ghimire, M. Wu, D. A. Browne, K. J. Schafer, M. B. Gaarde, and D. A. Reis, Solid-state harmonics beyond the atomic limit, *Nature (London)* **534**, 520 (2016).
- [57] M. Hohenleutner, F. Langer, O. Schubert, M. Knorr, U. Huttner, S. W. Koch, M. Kira, and R. Huber, Real-time observation of interfering crystal electrons in high-harmonic generation, *Nature (London)* **523**, 572 (2015).